Koufoudi, E., Ktenidou, O.-J., Cotton, F., Dufour, F., Grange, S. (2015): Empirical ground-motion models adapted to the intensity measure ASA 40. - *Bulletin of Earthquake Engineering*, *13*, 12, pp. 3625–3642.

DOI: http://doi.org/10.1007/s10518-015-9797-z

# Empirical Ground-Motion Models adapted to the intensity measure $ASA_{40}$

E. Koufoudi[1], O.-J. Ktenidou[2], F. Cotton[3], F. Dufour[1], S. Grange[1]

[1] *Univ. Grenoble Alpes, 3SR, F-38000 Grenoble, France*

[2] *ISTerre, Universite Grenoble 1, CNRS, F-38000 Grenoble, France*

[3] *GFZ Helmholtz Centre Potsdam GFZ German Research Centre for Geosciences, Potsdam, Germany*

eleni.koufoudi@3sr-grenoble.fr, +33 658566138

## Abstract

Relative Average-Spectral-Acceleration ($ASA_{40}$), a recently developed intensity measure, is defined as the average spectral pseudo-acceleration on the probable interval of evolution of the fundamental frequency of a structure. This article presents two ground motion prediction equations (GMPEs) appropriate for the prediction of $ASA_{40}$, using a pan-European strong motion database. Taking advantage of the strong correlation between the new intensity measure $ASA_{40}$ and the spectral pseudo-acceleration ($SA$), existing GMPEs predicting $SA$ can be adapted to predict $ASA_{40}$. The first GMPE used in this study is the modified version of a new generation ground motion model, ASB13. In order to decrease the high aleatory uncertainty (sigma) that accompanies predictions when using this modified model, a new model is developed for the prediction of $ASA_{40}$. Its range of applicability is for magnitudes $M_w$ from 5.5 to 7.6 and distances out to 200 km, it includes site amplification and it is applicable for a range of periods between 0.01 s and 4 s. The proposed model decreases the aleatory uncertainty by almost 15% with respect to the uncertainty of the modified ground motion model.

## Introduction

The Relative Average-Spectral-Acceleration ($ASA_r$) is a new intensity measure presented by De Biasio et al. (2014). Its main advantage over SA is its efficiency as an intensity measure appropriate for the structures that behave non-linearly. It takes into account the lengthening of the fundamental period due to progressive loss of stiffness caused by irreversible damage processes. The optimum value of frequency drop, R, of the structure was chosen as 40% by De Biasio et al. (2014). The prediction of the new intensity measure $ASA_{40}$ using Probabilistic Seismic Hazard Analysis (PSHA) would enforce its sufficiency as a robust intensity measure for the analysis of non-linearly behaving structures. However, since the performance of $ASA_{40}$ in terms of maximum interstorey drift is only slightly lower than that of *SA*, $ASA_{40}$ could also be used as a robust intensity measure when the behavior of the structure lies in the linear range. A key observation behind this study is that there is a good correlation between the classical intensity measure (*SA*) and the new intensity measure ($ASA_{40}$). This allows existing (GMPEs) for *SA* to predict $ASA_{40}$ as well.

RESORCE is the extended and updated version of the pan-European strong-motion databases compiled under the SHARE (**S**eismic **HA**rmonization in **E**urope) project (Akkar *et al.* 2014a). We use data from this databank to develop two GMPEs for the prediction of $ASA_{40}$. The most recent GMPE based on the RESORCE database for prediction of PGA and spectral ordinates is the model of Akkar et al. (2014b), which we will refer to here as ASB13. Here we modify it to predict $ASA_{40}$ by adjusting its coefficients according to the relation between *SA* and $ASA_{40}$. While the $ASA_{40}$ predictions are satisfactory, their uncertainty is relatively high with respect to the uncertainty of *SA* predictions, due to the scatter in the *SA*-$ASA_{40}$ correlations and the simplifications made in using the model.

In order to decrease this uncertainty, a new model was developed which is based directly on the new indicator and not on *SA* as a proxy. The functional form chosen includes magnitude, distance and $V_{s30}$ as its predictor variables. The uncertainty in the new model is lower and lies in the usual range of GMPE uncertainties, when they predict PGA and spectral ordinates (Akkar et al. 2014b; Akkar and Bommer 2010).

In this paper, we begin presenting the new intensity measure, ($ASA_r$), and the RESORCE database. We then modify the ASB13 functional form in order to predict $ASA_{40}$ and show the associated sigma values. We then calibrate a new functional form for the direct prediction of $ASA_{40}$ without $SA$ as a proxy. The associated sigma values are explored as well as predictions for a number of scenarios.

## Relative Average-Spectral Acceleration ($ASA_R$): the intensity measure

GMPEs were initially developed for the prediction of peak ground acceleration (PGA) and response spectral acceleration ($SA$) and recently are also developed to predict other quantities such as peak ground velocity (PSV), peak ground displacement (PSD), cumulative absolute velocity (CAV) EPRI (1988), etc. (Abrahamson and Silva 2008; Akkar et al. 2014b). The use of $SA$ is by definition the most efficient intensity measure for elastic single-degree-of-freedom (SDOF) systems. However, in the case of inelastic structural behaviour, $SA$ does not take into account the contribution of higher modes to the overall dynamic response or the lengthening of the fundamental period due to progressive loss of stiffness caused by irreversible damage processes. A structure-specific intensity measure has been developed by De Biasio et al. (2014) in order to consider the lengthening of the fundamental period of the structure. The new intensity measure is named Relative Average Spectral Pseudo-Acceleration ($ASA_r$). The term “relative” indicates the relation of the $ASA_r$ with the fundamental frequency of vibration of the structure.

For a frame structure according to Eurocode 8, as presented by De Biasio et al.

(2014), using events of high magnitudes in short distances from the same database, the standard deviation of the residuals of the maximum interstory drift ratio is 0.52 for PGA, 0.35 for *SA* and 0.28 for $ASA_{40}$. Thus, for the analysis of non-linearly behaving structures $ASA_{40}$ has considerably lower standard deviation with respect to PGA and *SA*.

The range of frequencies considered for the calculation of $ASA_r$ is between the fundamental frequency of the structure (as the upper bound) and the maximum expected "softened" frequency (as the lower bound) which is evaluated as a percentage of the fundamental value. For a structure approximated by a SDOF of fundamental frequency *f*, $ASA_r$ is defined for any seismic record as:

$$ASA_r(f) = \frac{1}{f(1-x_{f_1})} \int_{x_{f_1} \cdot f}^{f} S_{pa}(f_1, \xi)\, df_1 \quad (1)$$

*where*

*r* is the drop (as a percentage) of the structure's fundamental frequency,

$x_{f1} = 1-(r/100)$ is a factor accounting for the drop of the fundamental frequency,

*SA* is the spectral pseudo-acceleration for the given seismic record and

$\xi$ is the damping value.

The exact value of *r* depends on the non-linearity experienced by the structure, which depends on the intensity of the ground motion and on the design properties of the structure. Based on sensitivity analyses, an optimum value of 40% (i.e. $ASA_{40}$) was suggested by De Biasio et al. (2014). $ASA_{40}$ is the intensity measure used in this study. Hence the above equation can be rewritten as:

$$ASA_{40}(f) = \frac{2.5}{f} \int_{0.6 \cdot f}^{f} SA(f_1, \xi)\, df_1 \qquad (2)$$

The above formula can be simply rewritten in terms of period as:

$$ASA_{40}(T) = 2.5 \cdot T \int_{T}^{1.67T} \frac{SA(T_1, \xi)}{T_1^{2}}\, dT_1 \qquad (3)$$

**The RESORCE Strong Motion Database**

Our data come from the RESORCE strong-motion database, developed for the French SIGMA project (**S**e**I**smic **G**round **M**otion **A**ssessment, Akkar *et al.* 2014a). This database is the extended and updated version of the pan-European strong-motion databases compiled under the SHARE project (**S**eismic **HA**rmonization in **E**urope, Yenier *et al.* 2010). We chose a subset of the initial dataset based on certain criteria. Only sites with directly measured $V_{S30}$ values are included in order to minimize the epistemic uncertainty linked with site conditions. Earthquakes classified as aftershocks are also included, since any differences between spectral accelerations from main shocks and aftershocks are not significant (Douglas and Halldórsson 2010).

Akkar et al. (2014a) concluded that the available data are roughly unbiased for $M_w$ above 4.0 at distances out to 200 km. Since the intensity measure in which we are interested is structure-oriented, we specify the minimum magnitude to 4.5 instead of 4.0, after verifying that the volume of data is sufficient for the analysis. One of the main conclusions of Bommer et al. (2007) is that the empirical derivation of ground-motion prediction equations should be based on datasets extending at least one unit below the lower limit of magnitude considered in seismic hazard calculations. So if we want the GMPE's to be well calibrated for M>5.5 we need data for M>4.5. Following the majority of GMPEs, 200 km was selected as the upper limit of distances.

The distance metric we choose is the closest distance to the fault rupture ($R_{rup}$). Because rupture distance ($R_{rup}$) is not available for small events, we use $R_{rup}$ for events with Mw5.7 and above, and hypocentral distance ($R_{hypo}$) for earthquakes with Mw below 5.7. Point-source distances (i.e., hypocentral distance $R_{hypo}$ and epicentral distance $R_{epi}$) and extended-source distances (i.e., the horizontal distance to the closest point on the surface projection of the fault rupture $R_{JB}$, after Joyner and Boore, 1981, and rupture distance $R_{rup}$) respectively become equivalent for earthquakes for which the source dimensions are small or comparable with the uncertainty associated with the determination of epicentral/hypocentral coordinates. Akkar and Bommer (Earthq. Spectra, Feb. 2012, Figure 2) have compared a point-source distance ($R_{epi}$) and extended-source distance ($R_{JB}$) and show that for magnitudes below 5.7 these two measures are nearly identical. Such a simplification has been made in previous studies (e.g. Cotton et al., 2008). Recently, Yenier and Atkinson (2014) considered ground motions as originating from an equivalent point source and mimicked finite-fault effects by treating the motion as emanating from a virtual point. However, they considered differences between point-source and finite-fault ground-motions only for Mw>6.

Following suggestions by Akkar et al. (2014a), earthquakes recorded by only one station are not included in the subset, since they do not allow for sufficient determination of the event term and thus inflate the between-event variability in the models. In order not to further decrease the dataset, stations that recorded only one event were not eliminated. In order to allow this, we verified that the within-event variability did not increase significantly and hence the site terms are sufficiently captured. In order to focus only on shallow crustal earthquakes, following suggestions by Derras et al. (2013) and Laurendeau et al. (2013), recordings from events with focal depth less than 25 km are considered. Following the aforementioned exclusive criteria, the final dataset consists of 1092 recordings, with 86 events recorded by two stations, 41 events by three stations, 26 events by four stations and 79 events by five or more stations.

The distribution of the chosen dataset in terms of magnitude, distance and site classification after EC8 (Eurocode 8, CEN, 2004) is presented in Figure 1. Most records come from sites belonging to EC8 classes B and C, *i.e.* $180 \leq V_{S30} \leq 800$ m/s (soils and stiff soils). Only a few records come from soft soil (class D) or rock (class A) sites. Furthermore, earthquakes with magnitudes up to $M_w$ 6.4 are well represented, while for higher magnitudes data are more limited. Following the suggestion of Akkar et al. (2014a), we choose the range of periods in which to develop the $ASA_{40}$ prediction model: 0.01-4 s, i.e. frequencies from 0.25-100 Hz.

## Modifying an existing GMPE to predict $ASA_{40}$

For each of the records in our dataset we have calculated the $ASA_{40}$ for each one of the two horizontal components. Then we calculated their geometric mean in the range between 0.01 to 4 s with a time step of 0.01 s. Figure 2 shows the relation between $SA$ and $ASA_{40}$ in natural log scale for all data points. Data is shown at three characteristic periods that are of interest for engineered structures, namely 0.2, 0.6 and 1 s and two additional longer periods, 2 and 3.5 s, for the sake of completeness. The relation between the natural logarithm of the two intensity measures is linear, with a coefficient of correlation that is almost equal to 1. Figure 3 presents the $ASA_{40}$ calculated for the dataset as a function of distance for magnitudes equal to 4.5, 6.0 and 7.3, at periods 0.2, 0.6, 1, 2 and 3.5 s. The trend of $ASA_{40}$ with distance is similar to the trend that *SA* follows with distance, as expected due to their high correlation. The magnitude scaling (Figure 4) is also similar to the magnitude scaling of *SA*.

Based on these observations, we infer that we can use the typical formulations of a GMPE made to predict *SA* in order to predict $ASA_{40}$. First we use an existing functional form developed for the RESORCE dataset. The most recent GMPE based on this database is ASB13. It models ground motion scaling in terms of magnitude, distance, $V_{s30}$ and style-of-faulting (SoF), using the random effects procedure of Abrahamson and Youngs (1992). It predicts *SA* at periods from 0.01 to 4 s. The coefficients are adjusted according to the type of distance R used (the Joyner-Boore distance $R_{JB}$, the hypocentral distance $R_{hypo}$ and the closest distance to the fault rupture $R_{rup}$). The functional form is given in Eqs. (4) - (6):

$$\ln(SA) = \ln\left[SA_{REF}(M_w, R, SoF)\right] + \ln\left[S(V_{s30}, PGA_{REF})\right] + \varepsilon\sigma_t \tag{4}$$

Where

$$\ln(SA_{REF}) = \begin{cases} a_1 + a_2(M_w - c_1) + a_3(8.5 - M_w)^2 + [a_4 + a_5(M_w - c_1)]\ln\left(\sqrt{R^2 + a_6^2}\right) + a_8F_N + a_9F_R \\ \quad for\ M_w \leq c_1 \\ a_1 + a_7(M_w - c_1) + a_3(8.5 - M_w)^2 + [a_4 + a_5(M_w - c_1)]\ln\left(\sqrt{R^2 + a_6^2}\right) + a_8F_N + a_9F_R \\ \quad for\ M_w > c_1 \end{cases} \tag{5}$$

and

$$\ln(S) = \begin{cases} b_1(T)\ln\left(V_{s30}/V_{REF}\right) + b_2(T)\ln\left\{\left[PGA_{REF} + c\left(\frac{V_{s30}}{V_{REF}}\right)\right] / \left[PGA_{REF} + c\left(\frac{V_{s30}}{V_{REF}}\right)\right]\right\} \\ \quad for\ V_{s30} < V_{REF} \\ b_1(T)\ln\left(\frac{V_{s30}}{V_{REF}}\right) for\ V_{REF} \le V_{s30} \le V_{CON} \\ b_1(T)\ln\left(\frac{V_{CON}}{V_{REF}}\right) for\ V_{s30} > V_{CON} \end{cases} \tag{6}$$

As explained by Akkar et al. (2014b), in equations (4)-(6) the median spectral acceleration *ln(SA)* is computed by modifying the reference ground-motion model *ln(SA<sub>REF</sub>)* through the nonlinear site amplification function *ln(S)*. The estimator parameters of the reference ground-motion model are the moment magnitude, $M_w$, source-to-site distance measure, R, for which $R_{JB}$, $R_{epi}$, $R_{hypo}$ are used for different cases; and the style-of-faulting dummy variables. The parameters $F_N$ and $F_R$ are unity for normal and reverse faults, respectively, and zero otherwise. In the reference ground-motion model the parameter $c_1$ is the hinging magnitude, taken as $M_w$ 6.75. The total aleatory variability of the model is given by σ that is composed of within-event ($\varphi$) and between-event ($\tau$) standard deviations, following the nomenclature of Alatik et al. (2010) of the $deltaW_{es}$ and $deltaB_e$ residuals, respectively where the subscripts e and s refer to event and station. The period-dependent estimator parameters of the nonlinear site function (i.e., $b_1$ (T) and $b_2$ (T)) as well as *c* (2.5) and *n* (3.2) in the model of Akkar et al. (2014b) are directly adopted from the Sandıkkaya *et al.* (2013a) model. The reference $V_{S30}$ ($V_{REF}$) is 750m/s in the nonlinear site model and $V_{CON}$=1000m/s that stands for the limiting $V_{S30}$ after which the site amplification is constant. The reference rock site PGA ($PGA_{REF}$) is calculated from the reference ground-motion model in Eq. (4).

Douglas et al. (2014) compared the style of faulting factors for the five GMPEs derived from the RESORCE database (Akkar et al., 2014a). These ratios are generally quite close to unity (i.e., the rupture mechanism has little or no effect on spectral accelerations). This observation is in line with findings from previous studies, including some associated with the NGA models. Moreover, the RESORCE database is not well adapted to the analysis of style of faulting effects, because of the poorly balanced number of reverse, strike-slip, and normal events in the database. For these reasons the style of faulting was not considered in the modified model with the scope of simplification.

To adjust the coefficients of the existing model so as to predict $ASA_{40}$, a linear regression analysis was performed along the periods of interest between the natural logarithm of the two intensity measures. The subset of events used herein differs from the dataset used by Akkar et al. (2014b) since in the selection of events, we use hypocentral distance for events with $M_w$<5.7 and rupture distance for larger events. The coefficients of ASB13 model are grouped in three categories according to the type of distance. However, using either group of coefficients, $R_{hypo}$ or $R_{JB}$, the difference in the results in terms of standard deviation is insignificant. Thus, we use the coefficients corresponding to hypocentral distance $R_{hypo}$ because they are available for all events.

Figure 5 shows the aleatory uncertainty (sigma value) corresponding to the modified ASB13 model, which is 15%-20% higher compared to the sigma of the original Akkar et al. (2014b) when predicting *SA*. This increase is expected due to the scatter in the correlation between the two intensity measures. Additionally, a small deviation is introduced due to the differences in the subsets used in the two studies, the type of distance metric used, the group of coefficients chosen, and the dismiss of the style-of-faulting. Despite this increase in sigma compared to the original model, we conclude that the modified model can be used for the prediction of $ASA_{40}$ despite that the standard deviation found is higher than the values of uncertainty in typical GMPEs that predict *SA*, such as the NGA-West2 and the pan-European models (e.g Abrahamson and Silva 2008; Akkar et al. 2014b; Akkar and Bommer 2010, Bindi et al. 2010; Boore and Atkinson 2008). The predictions are sufficiently accurate, especially for periods shorter than 1 s, which is the range of periods that is most interesting from a structural engineering point of view.

## Creating a new GMPE to predict $ASA_{40}$

We first used an existing functional form appropriate for predicting *SA*, and adjusted it based on the correlation between *SA* and $ASA_{40}$. The uncertainty introduced from that model was higher than the uncertainties found in the literature, therefore now we create a new model that predicts $ASA_{40}$ directly. The chosen functional form takes into account magnitude, distance and site conditions dependency, it is simplified with respect to ASB13, so as to only include basic scaling features of next generation GMPEs for which we have adequate knowledge. The seven coefficients of the model are regressed using the random effect method of Abrahamson and Youngs (1992) and the uncertainty is broken into the within-event and (φ) and between-events (τ) standard deviations (Al Atik et al. 2010).

The functional form of the model is given in Eqs (7)-(10):

$$\ln\left(ASA_{40,es}\right) = F_{M_i} + F_{D_{ij}} + F_{S_j} + \delta W_{es} + \delta B_e \tag{7}$$

where:

$$F_{M_e} = b_1 \cdot M_w + b_2 \cdot M_w{}^2 \tag{8}$$

$$F_{D_{es}} = (b_3 + b_4 \cdot (M_w - 6)) \cdot \ln(R + 10) + b_5 \cdot R \tag{9}$$

$$F_{S_s} = b_6 \cdot \ln\left(\frac{V_{S30}}{800}\right) + b_7 \tag{10}$$

Figure 6 shows predictions for *ASA40* with distance out to 200 km, for magnitudes equal to 5, 6 and 7, at periods 0.2, 0.6, 1, 2 and 3.5 s. Figure 7 shows *ASA40* predictions with magnitude for distances equal to 10, 30 and 100 km respectively. All results are shown for a reference rock with $V_{S30}$=800 m/s. Figure 8 shows *ASA40* as a function of period for different distances (10, 30, and 100 km) and different magnitudes ($M_w$ 5, 6, and 7), while Figure 9 shows results for different $V_{S30}$ values (180, 360, and 800 m/s, i.e. the limits between EC8 site classes A through D). The dependencies on *ASA40* with the explanatory variables $M_w$ and R and as a function of period follow typical GMPE tendencies (Akkar et al. 2014b; Akkar and Bommer 2010).

Figures 10 through 12 show residual plots for *ASA40* at periods of 0.2, 0.6, 1, 2 and 3.5 s with respect to magnitude, distance, and $V_{S30}$. The average residuals (black circles) are shown for bins of each independent variable along with their standard deviation. The between-events residuals (delta$B_e$) do not show any significant trends with magnitude (Figure 10), while the within-event residuals (delta$W_{es}$) are well centered through all distances (Figure 11). These observations indicate that the proposed model is well balanced and predicts *ASA40* well without systematic bias as to the predictor variables. Figure 12 shows that predictions are unbiased for EC8 site classes A, B, C and D, while the model underestimates rock motion (for $V_{S30}$>1100 m/s) at all periods. This is most probably because data in this $V_{S30}$ range are sparse and poorly distributed. Table 1 presents the period-dependent coefficients for some selected periods.

Figure 13 shows the variation of the between-event (τ), within-event (φ), and total (σ) standard deviation values for the proposed model. The results support the observation of Strasser *et al*. (2009) that the φ component of the uncertainty is much larger than the τ. The standard deviations increase with period above 0.5 or 1 s. Within the period range of engineering interest (below 1 s) the standard deviation is almost constant (around 0.4, 0.6 and 0.7 for τ, φ, and σ, respectively) and similar to the values of uncertainty in typical GMPEs that predict *SA*, such as the NGA-West2 and the pan-European models (e.g Abrahamson and Silva 2008; Akkar et al. 2014b; Akkar and Bommer 2010; Bindi et al. 2010; Boore and Atkinson 2008; and Derras et al 2013).

Furthermore, some sensitivity analyses were performed in order to test the robustness of the model. We repeated our analyses excluding stations that recorded only one event, as well as events that were recorded by less than 3 stations. The effect on standard deviation was insignificant, meaning that the source and site terms were sufficiently captured. Hence, in order not to further reduce our subset, we only exclude events recorded at less than 2 stations.

Even though we used the same dataset in both cases to predict $ASA_{40}$, several simplifications were made when using the modified ASB13 model. As expected, the uncertainty of the new model is lower than the uncertainty of the modified ASB13 model in all periods. The new model has a simpler functional form with fewer coefficients to be calibrated, allowing better stability.

## Conclusions

Here we present models appropriate for the prediction of a new intensity measure related to structural behavior called, the Relative Average Pseudo-Acceleration ($ASA_{40}$). Our data come from the RESORCE Strong Motion Databank. We observe that, in log space, $ASA_{40}$ has a linear relation with $SA$ as expected from its definition. Based on this correlation, an existing GMPE intended for the prediction of spectral ordinates is modified to predict $ASA_{40}$. We choose Akkar et al. 2014b (ASB13), which is based on the same database, and we adjust it according to the correlation of the two intensity measures at each period in our range of interest (0.01 to 4 s). Although acceptable, the uncertainty in the prediction of $ASA_{40}$ is higher with respect to the uncertainty in the prediction of $SA$. This is likely due to the scatter in the $SA$ - $ASA_{40}$ correlation, the differences in the choice of subset, and the simplifications made to the original model.

Thus, a new GMPE is developed using the same dataset, aiming to directly predict $ASA_{40}$ without $SA$ as a proxy. The new model predicts $ASA_{40}$ without bias as to magnitude or distance, for EC8 site classes A through D. The aleatory uncertainty is now lower and its components $\tau$, $\varphi$, and $\sigma$ are similar to that of typical GMPEs appropriate for the prediction of spectral ordinates and decreased with respect to the uncertainty when adjusting the already existing GMPE, ASB13.

The use of the $ASA_{40}$ could be particularly advantageous when non-linear behavior of a structure is expected, due to the location and/or structural design. However, when the behavior of the structure lies in the linear range, the performance of $ASA_{40}$ in terms of maximum interstorey drift is slightly lower than that of *SA*. This is why $ASA_{40}$ could also be used in the framework of Probabilistic Seismic Hazard Analysis (PSHA), and therefore needs to be estimated in bins of magnitude and distances that do not necessarily lead to non-linear structural behavior. Thus, for the calibration of the GMPEs used herein for the prediction of $ASA_{40}$, we extended the database to lower values of magnitude and higher values of distance with respect to the high-damage bin (e.g. $M_w>5.5$ and R<100 km).

In the context of risk assessment, vulnerability parameters must be taken into account in order to estimate vulnerability indicators. Although the GMPE introduced here could be used directly to provide a rough estimate of a vulnerability indicator such as interstorey drift, the latter strongly depends on vulnerability parameters (relative importance of the few first eigenmodes, ductility factor, etc.), which are not accounted for in the present GMPE. Therefore, for an accurate analysis of a given structure, we recommend the development of a GMPE to specifically estimate vulnerability indicators such as interstorey drift.

## Acknowledgements

The work presented in this article has been developed within the French SIGMA project (Seismic ground motion assessment, http://projet-sigma.com). The electronic supplements of Akkar et al. (2014b) were used for the ASB13 model. Special thanks to R. Kamai for her regression code and to M. De Biasio for the helpful discussion.

## References


Abrahamson, N.A., Silva, W., 2008. Summary of the Abrahamson & Silva NGA ground-motion relations. *Earthquake Spectra* **24**: 67-97

Abrahamson, N.A., Youngs, R.R., 1992. A stable algorithm for regression analyses using the random effects model. *Bulletin of the Seismological Society of America* **82**:505-510.

Akkar, S., Bommer, J.J., 2010. Empirical equations for the prediction of PGA, PGV and spectral accelerations in Europe, the Mediterranean and the Middle East. *Seismological Research Letters* **81:**195-206.

Akkar, S.; Sandıkkaya, M.; Şenyurt, M.; Azari Sisi, A.; Ay, B.; Traversa, P.; Douglas, J.; Cotton, F.; Luzi, L.; Hernandez, B.; Godey, S., 2014a. Reference Database for Seismic Ground-Motion in Europe (RESORCE). *Bulletin of Earthquake Engineering* Vo.. 12(1), pp. 311-339.

Akkar, S., Sandikkaya, M.A., Bommer, J.J., 2014b. Empirical ground-motion models for point- and extended-source crustal earthquake scenarios in Europe and the Middle East. *Bulletin of Earthquake Engineering* **12**:359-387.

Akkar, S., Sandikkaya, M.A., Bommer, J.J., 2014b. Erratum to: Empirical ground-motion models for point- and extended-source crustal earthquake scenarios in Europe and the Middle East. *Bulletin of Earthquake Engineering* doi: 10.1007/s10518-013-9508-6.

Al Atik, L., Abrahamson, N.A., Bommer, J.J., Scherbaum, F., Cotton, F., Kuehn, N. 2010. The variability of ground-motion prediction models and its components. *Seismological Research Letters* **81:**783-793.

Atkinson, M., Boore, D., 2003. Empirical ground-motion relations for subductionzone earthquakes and their application to Cascadia and other regions. *Bulletin of Seaismological Society of America,* **93:**1703-1729.

Bindi, D., Luzi, L., Massa, M., Pacor, F. 2010. Horizontal and vertical ground motion prediction equations derived from the Italian Accelerometric Archive (ITACA). *Bulletin of Earthquake Engineering* **8**:1209-1230.

Bommer, J.J. & S. Akkar (2012). Consistent source-to-site distance metrics in ground-motion prediction equations and seismic source models for PSHA. *Earthquake Spectra* 28(1), 1-15

Bommer, J.J, Stafford, P.J, Alarcon, J.E, Akkar, S., 2007. The influence of magnitude range on empirical ground-motion prediction. *Bulletin of the Seismological Society of America, Vol. 97, No. 6, pp. 2152–217.*

Boore, D.M., Atkinson, G.M., 2008. Ground-motion prediction equations for the average horizontal component of PGA, PGV, and 5%-damped PSA at spectral periods between 0.1s and 10.0s. *Earthquake Spectra* **24**:99-138.

Comité Européen de Normalisation (CEN), 2004. Eurocode 8, Design of structures for earthquake resistance—part 1: General rules, seismic actions and rules for buildings. *European Standard NF EN* 1998-1, Brussels.

Cotton F., Pousse G., Bonilla F., and Scherbaum F., 2008. On the Discrepancy of Recent European Ground-Motion Observations and Predictions from Empirical Models: Analysis of KiK-net Accelerometric Data and Point-Sources Stochastic Simulations. *Bulletin of the Seismological Society of America* vol. 98 no. 5 2244-2261.

De Biasio, M., Grange, S., Dufour, F., Allain, F., Petre-Lazar, I., 2014. A simple and efficient intensity measure accounting for non-linear structural behavior. *Earthquake Spectra (Accepted).*

Derras, B., Bart, P.Y., Cotton, F., 2013. Towards fully data driven ground-motion prediction models for Europe. *Bulletin of Earthquake Engineering.*

Douglas J, Akkar S, Ameri G, Bard P-Y, Bindi D, Bommer JJ, Bora SS, Cotton F, Derras B, Hermkes M, Kuehn NM, Luzi L, Massa M, Pacor F, Riggelsen C, Sandikkaya MA, Scherbaum F, Stafford PJ, Traversa Pet al., 2014. Comparisons among the five ground-motion models developed using RESORCE for the prediction of response spectral accelerations due to earthquakes in Europe and the Middle East. *Bulletin of Earthquake Engineering*, Vol: 12, Pages: 341-358, ISSN: 1570-761X

Douglas J., Halldórsson B., 2010. On the use of aftershocks when deriving ground-motion prediction equations. *9th U.S. National and 10th Canadian Conference on Earthquake Engineering (9USN/10CCEE) p.* Paper no. 220.

EPRI, 1988. A criterion for determining exceedance of the operating basis earthquake. EPRI NP-5930. Electric Power Research Institute, USA.

Joyner, W.B, Boore, D.M, 1981. Peak horizontal acceleration and velocity from strong-motion records including records from the 1979 Imperial Valley, California, earthquake. *Bulletin of the Seismological Society of America,* **71**:2011-2038

Laurandeau, A., Cotton, F., Ktenidou, O.-J., Bonilla, L-F., Hollender, F., 2013. Rock and stiff-soil site amplification: Dependency on $V_{s30}$ and Kappa ($\kappa_0$). *Bulletin of the Seismological Society of America, Vol. 103, No. 6, pp -.*

Sandikkaya, M.A., Akkar, S., Bard, P.Y., 2013a. A nonlinear site amplification model for the next Pan-European ground-motion prediction equations. *Bulletin of the Seismological Society of America, 103(1), 19-32.*

Strasser, F.O., Abrahamson, N.A., Bommer, J.J., 2009. Sigma: Issues, insights, and challenges. *Seismological Research Letters* **80**:40-56.

Yenier, E., Atkinson, G.M., 2014. Equivalent Point-Source Modeling of moderate to large magnitude earthquakes and associated ground-motion saturation effects. *Bulletin of the Seismological Society of America,* **104**:1458-1478.

Yenier, E., Sandıkkaya, M.A., Akkar, S., 2010. Report on the fundamental features of the extended strong motion databank prepared for the SHARE project. pp. 44. Deliverable 4.1 of Seventh Framework Programme Project Seismic Hazard Harmonization in Europe (SHARE), 34 pages, Ankara.

**List of Symbols**

$ASA_r$ = Relative Average Spectral Pseudo-Acceleration

$ASA_{40}$ = Relative Average Spectral Pseudo-Acceleration with 40% frequency drop

$SA$ = Spectral Acceleration

$M_w$ = Moment Magnitude

R= Distance

$R_{rup}$ = Rupture Distance

$R_{hypo}$ = Hypocentral Distance

$R_{JB}$ = Distance Joyner and Boore

$R_{epi}$ = Epicentral Distance

$V_{S30}$ = Average Shear Wave Velocity in the top 30 m of soil

SoF= Style of Faulting

PGA = Peak Ground Acceleration

PSV = Peak Ground Velocity

PSD = Peak Ground Displacement

CAV = Cumulative Average Velocity

SDOF = Single Degree of Freedom System

$x_{f1}$ = factor accounting for the drop of the fundamental frequency

r = drop (as a percentage) of the structure's fundamental frequency

$\xi$ = the damping value

$\sigma$ = Total Variability

$\phi$ = Within event variability

$\tau$ = Between events variability

$deltaB_e$ = Between events residuals

$deltaW_{es}$ = Within event residuals

e = event

s = station

**Table 1.** Period-dependent coefficients of the ground motion model for some selected periods.

| Period (s) | $b_1$ | $b_2$ | $b_3$ | $b_4$ | $b_5$ | $b_6$ | $b_7$ |
|---|---|---|---|---|---|---|---|
| 0,02 | 1,8237 | -0,2659 | -1,4000 | 0,5770 | -0,0032 | -0,3047 | 3,2487 |
| 0,04 | 1,2200 | -0,2323 | -1,2000 | 0,6188 | -0,0064 | -0,2343 | 5,1787 |
| 0,06 | 1,2549 | -0,2355 | -1,2000 | 0,6098 | -0,0076 | -0,1853 | 5,3709 |
| 0,08 | 1,6375 | -0,2633 | -1.0000 | 0,5915 | -0,0106 | -0,1493 | 3,6489 |
| 0,1 | 1,9820 | -0,2759 | -1.0000 | 0,5462 | -0,0107 | -0,1511 | 2,1744 |
| 0,2 | 3,5978 | -0,34089 | -1.0000 | 0,3650 | -0,0085 | -0,3606 | -5,2825 |
| 0,3 | 4,6598 | -0,3978 | -1,2000 | 0,3030 | -0,0035 | -0,5494 | -9,3360 |
| 0,4 | 5,2591 | -0,4395 | -1,2000 | 0,3038 | -0,0021 | -0,6851 | -11,7751 |
| 0,5 | 5,8095 | -0,4749 | -1,2000 | 0,2952 | -0,0010 | -0,8001 | -14,0737 |
| 1,0 | 6,7347 | -0,5222 | -1,2000 | 0,2709 | 0,0023 | -0,9387 | -19,0464 |
| 2,0 | 7,4114 | -0,5749 | -0,8000 | 0,3143 | -0,0013 | -0,8779 | -23,7117 |
| 3,0 | 7,3213 | -0,5396 | -0,8000 | 0,2736 | -0,0018 | -0,8401 | -25,3802 |
| 4,0 | 7,1924 | -0,5009 | -0,8000 | 0,2456 | -0,0025 | -0,8193 | -25,6974 |

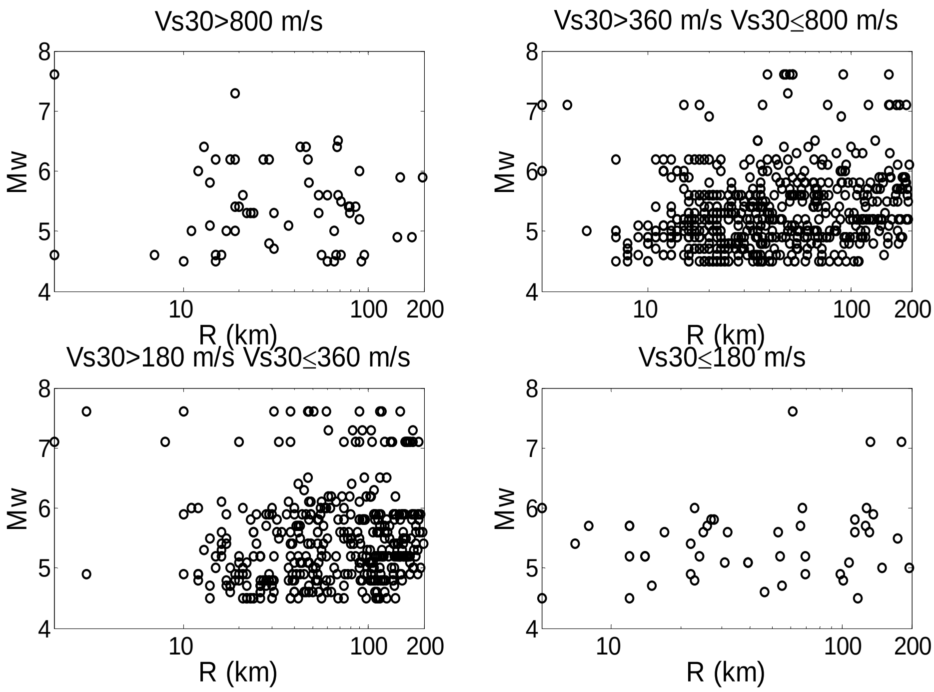


**Figure 1:** Distribution of the data used in terms of magnitude, distance and site classification after EC8.

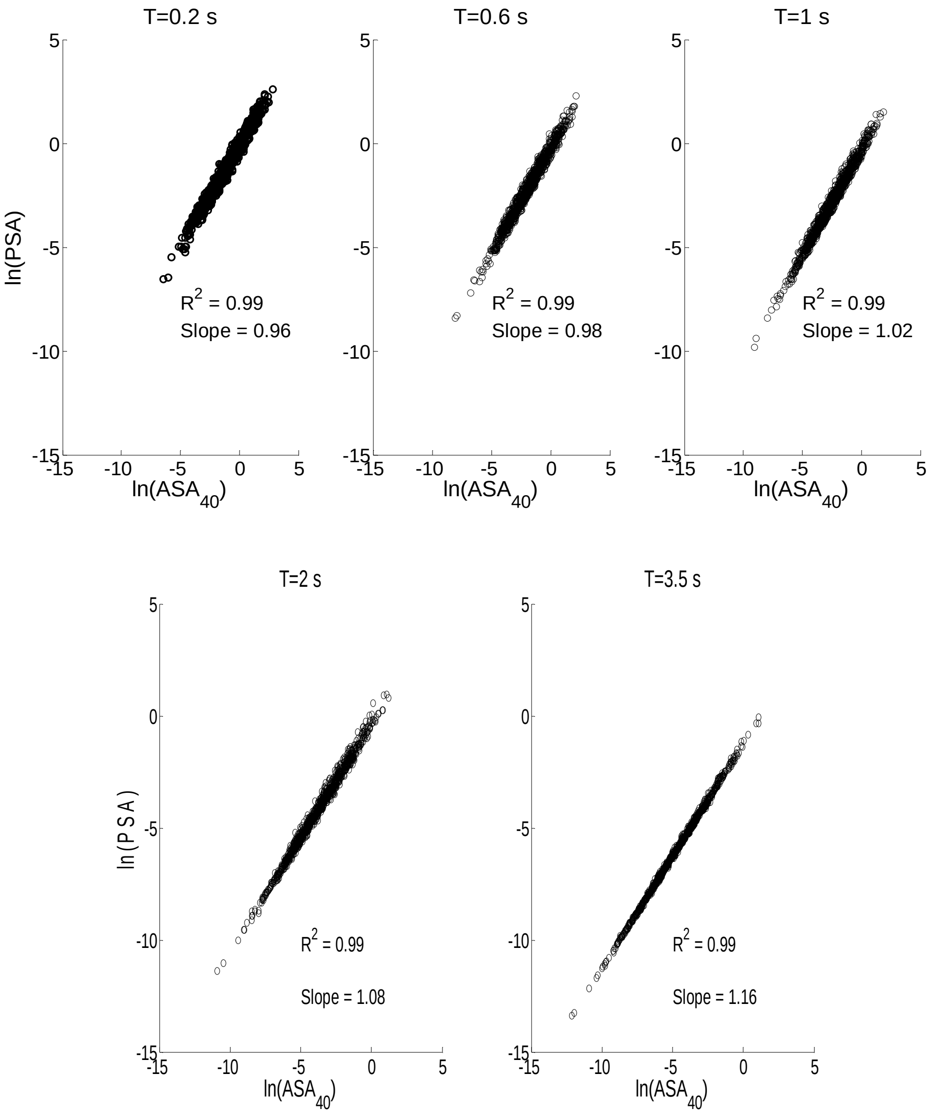


**Figure 2:** Correlation between the natural logarithm of SA and the natural logarithm of $ASA_{40}$ for 7 at periods 0.2 s, 0.6 s, 1 s, 2 s and 3.5 s.

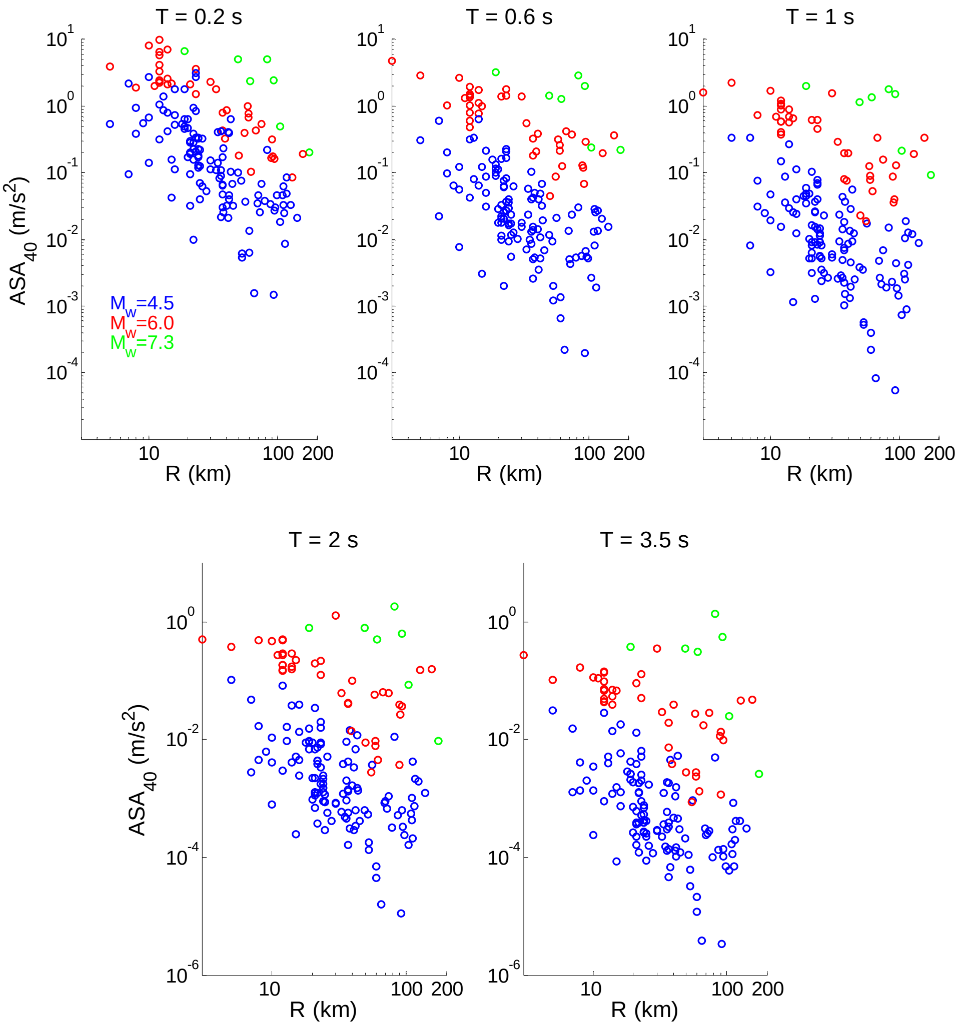


**Figure 3:** Distance dependence of calculated ASA40 values in the dataset for magnitude values of Mw4.5, Mw6.0, and Mw7.3 7 at periods 0.2 s, 0.6 s, 1 s, 2 s and 3.5 s.

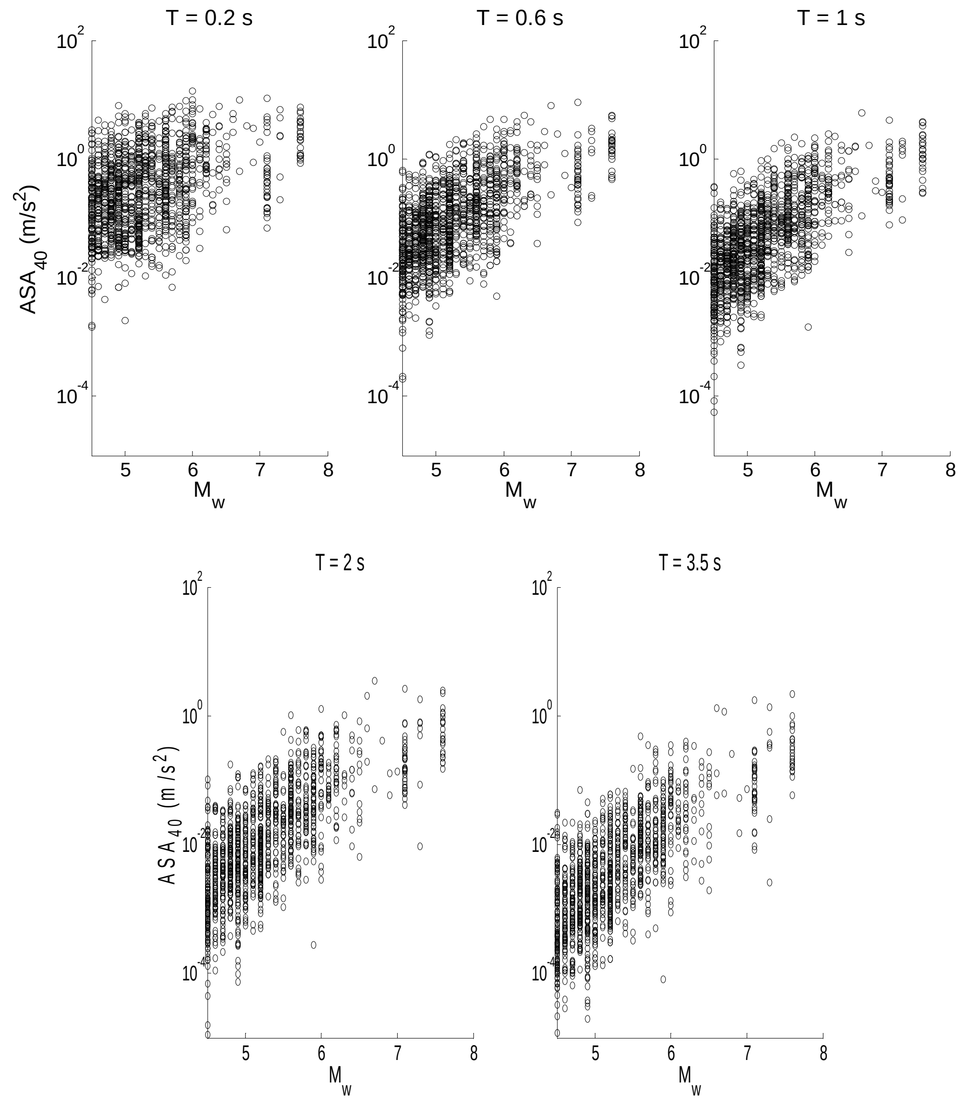


**Figure 4:** Magnitude dependence of *$ASA_{40}$* for periods 7 at periods 0.2 s, 0.6 s, 1 s, 2 s and 3.5 s.

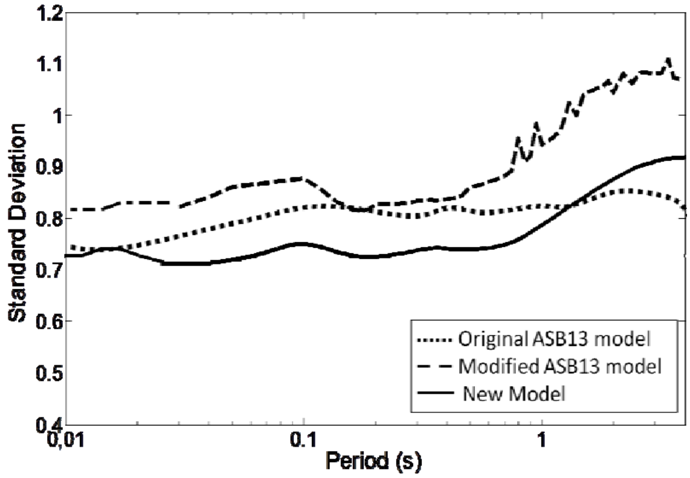


**Figure 5:** Standard deviation of $ASA_{40}$ using the modified ASB13 model and the new model and standard deviation of SA using the original ASB13 model.

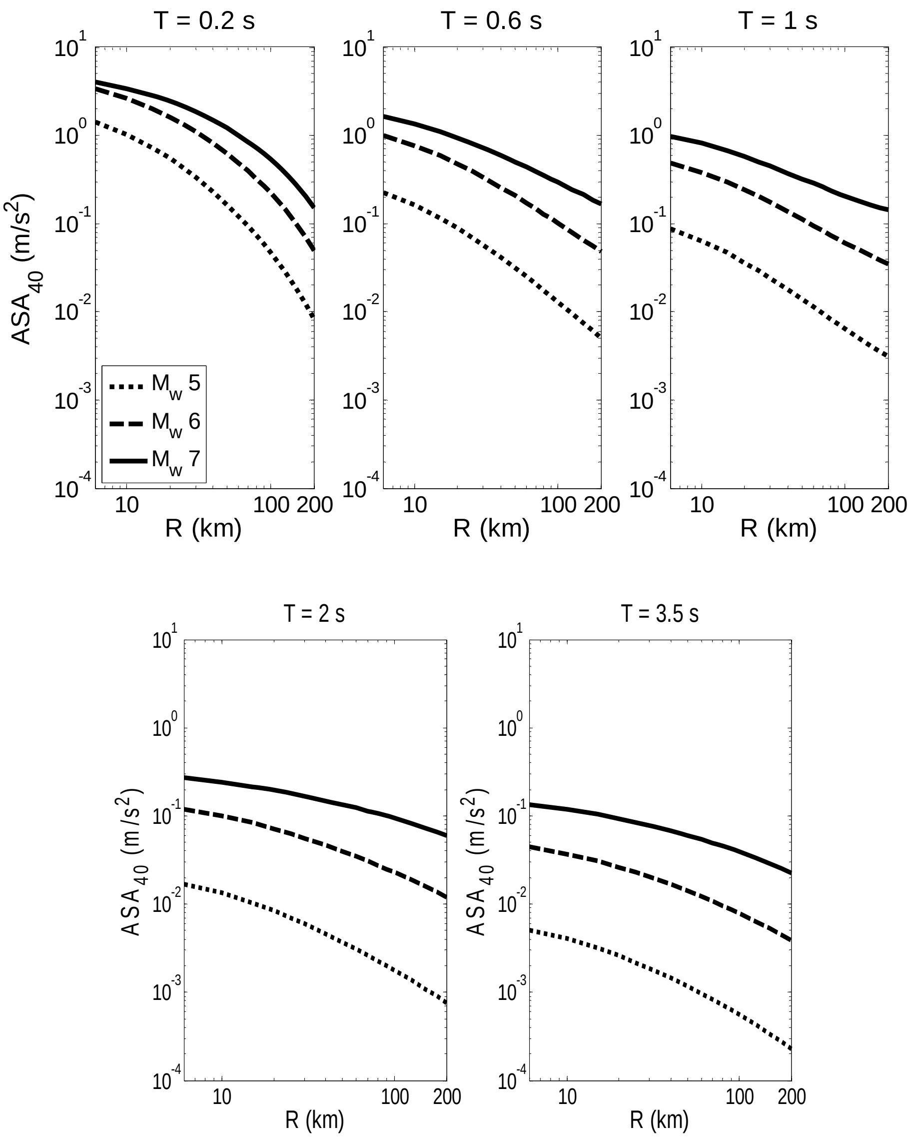


**Figure 6:** *$ASA_{40}$* distance scaling for $V_{s30}$=800 m/s and for $M_w$ equal to 5, 6 and 7 at periods 0.2 s, 0.6 s, 1 s, 2 s and 3.5 s.

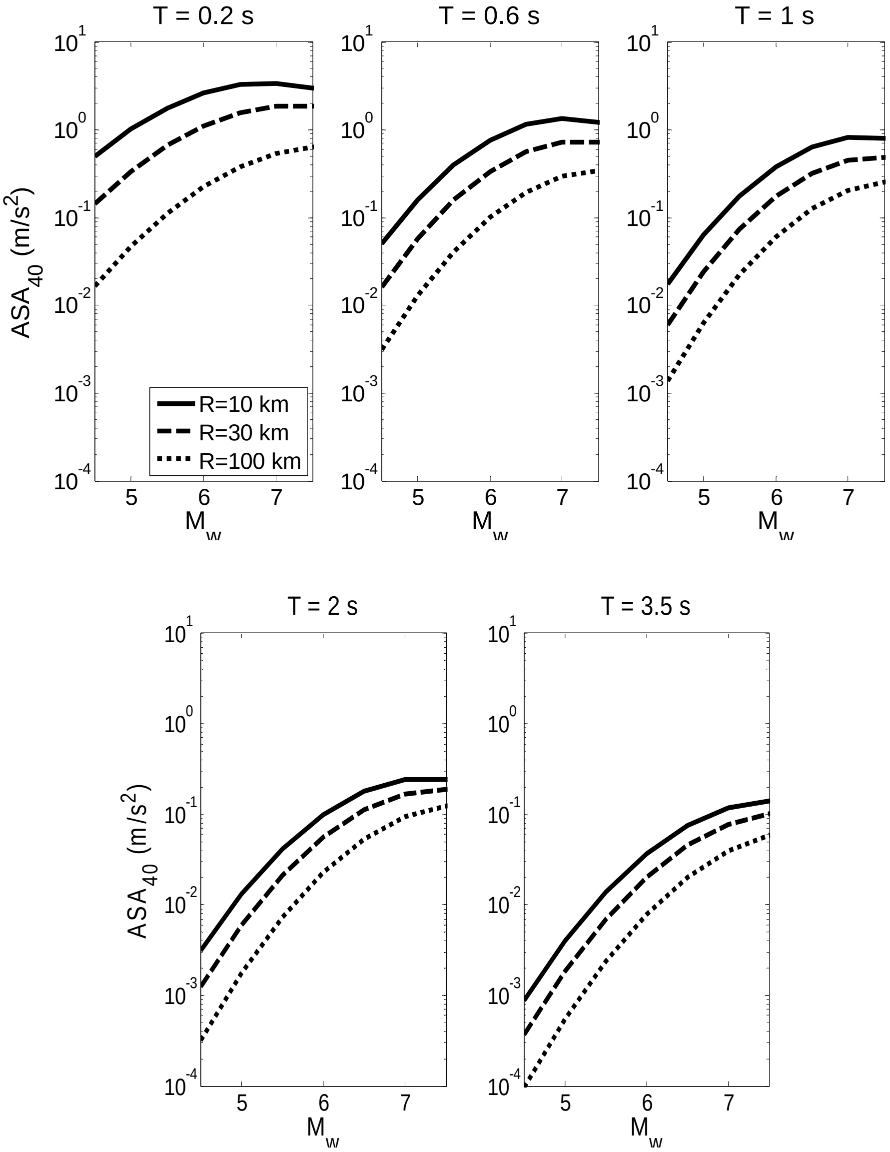


**Figure 7:** *$ASA_{40}$* magnitude scaling for $V_{s30}$=800 m/s and for R equal to 10, 30, and 100 km at periods 0.2 s, 0.6 s, 1 s, 2 s and 3.5 s.

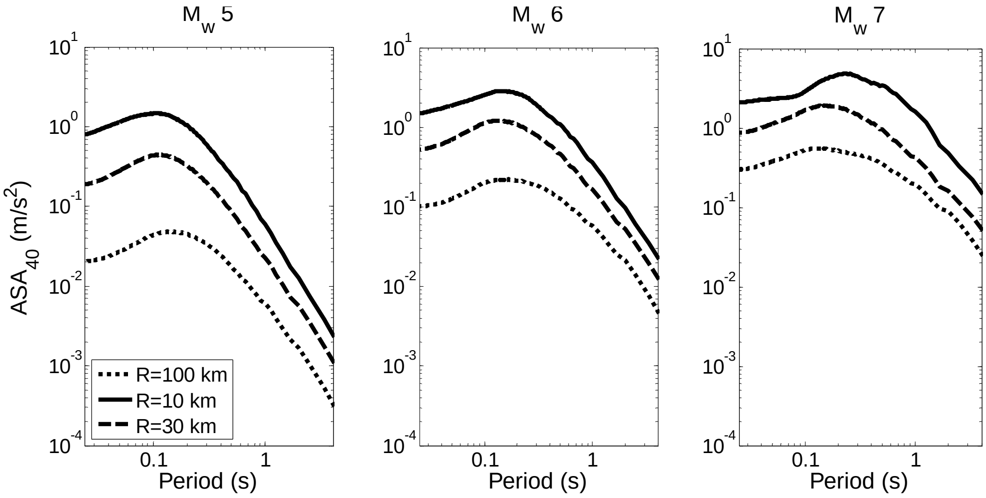


**Figure 8:** Scaling of $ASA_{40}$ with period for R equal to 10, 30, and 100 km and $M_w$ 5 6 7.

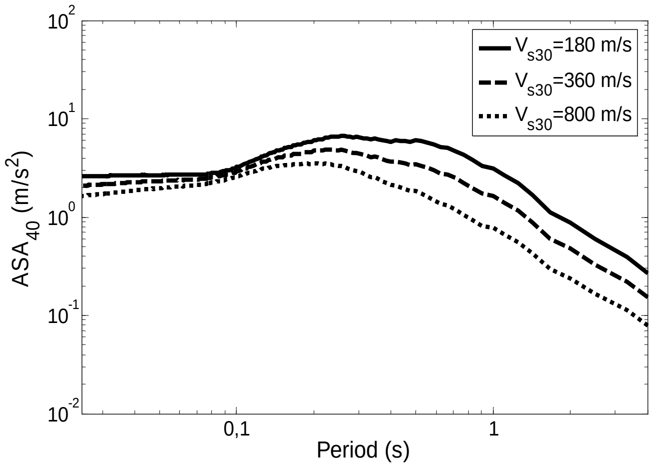


**Figure 9:** Scaling of $ASA_{40}$ with period for $V_{s30}$= 180, 360, and 800 m/s, R equal to 10 km and $M_w$ 7.

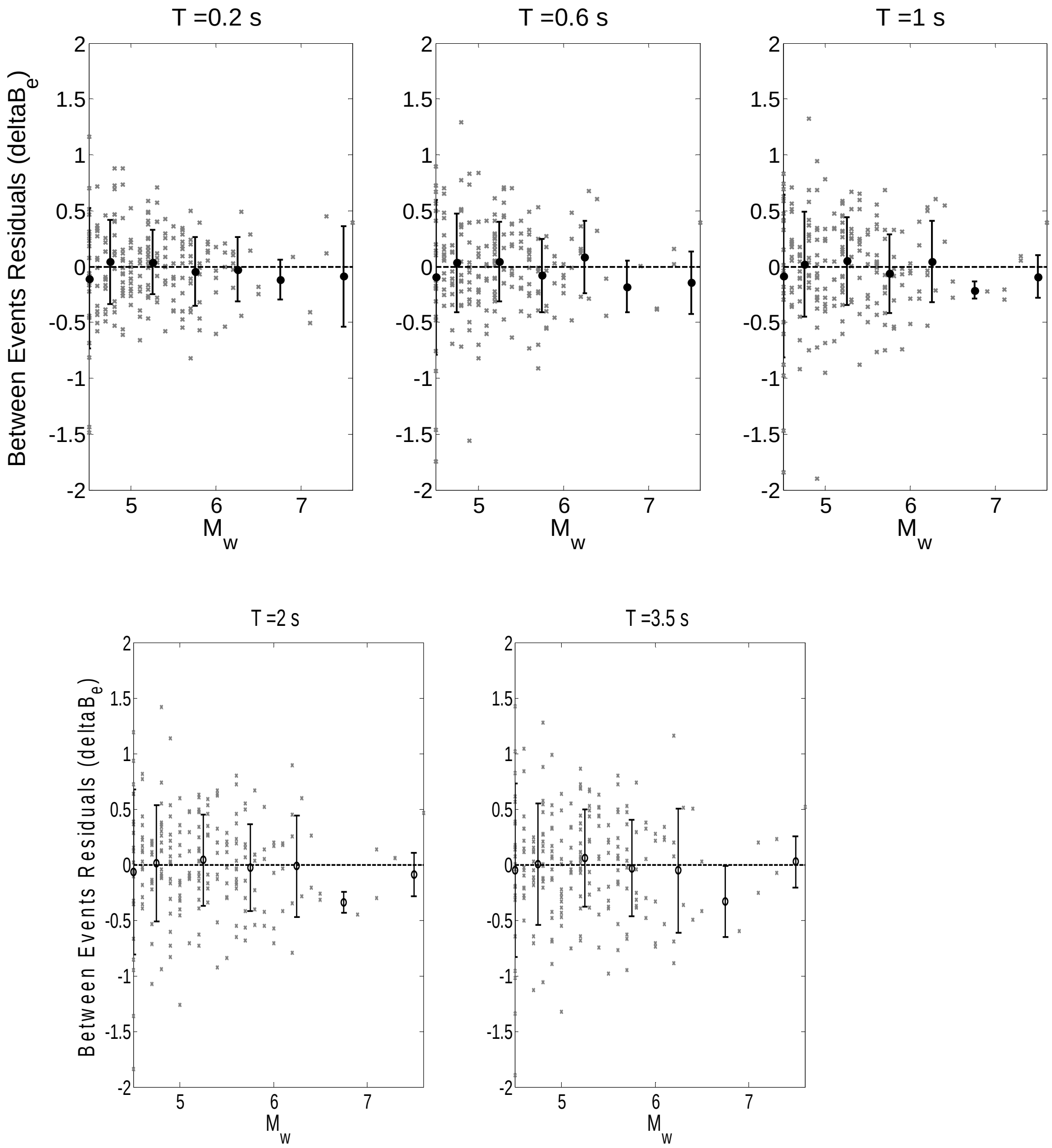


**Figure 10:** Between-event residuals (deltaB$_e$) and binned averages with respect to magnitude at periods 0.2 s, 0.6 s, 1 s, 2 s and 3.5 s.

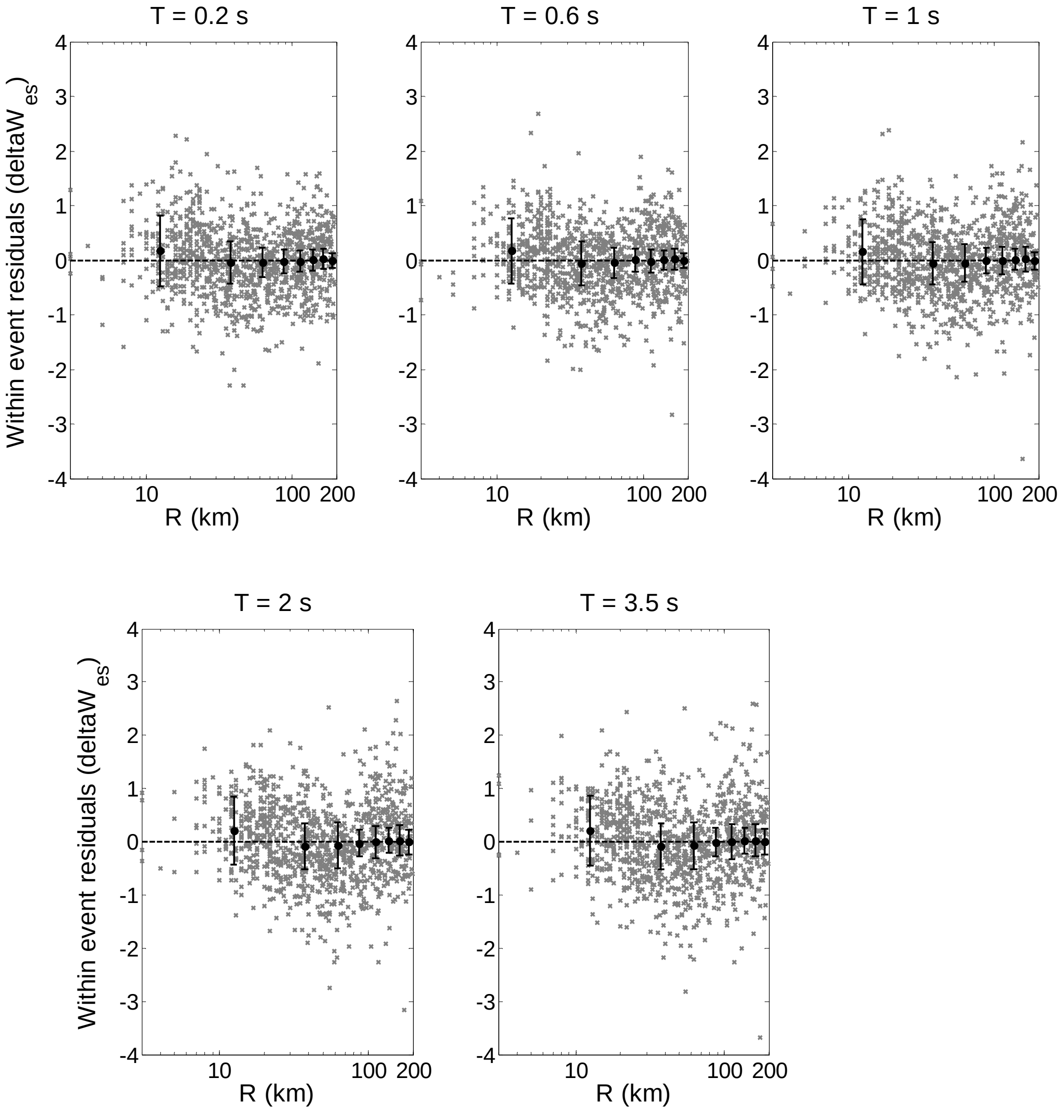


**Figure 11:** Within-event residuals (delta$W_{es}$) and binned averages with respect to distance at periods 0.2, 0.6, 1 s, 2 s and 3.5 s.

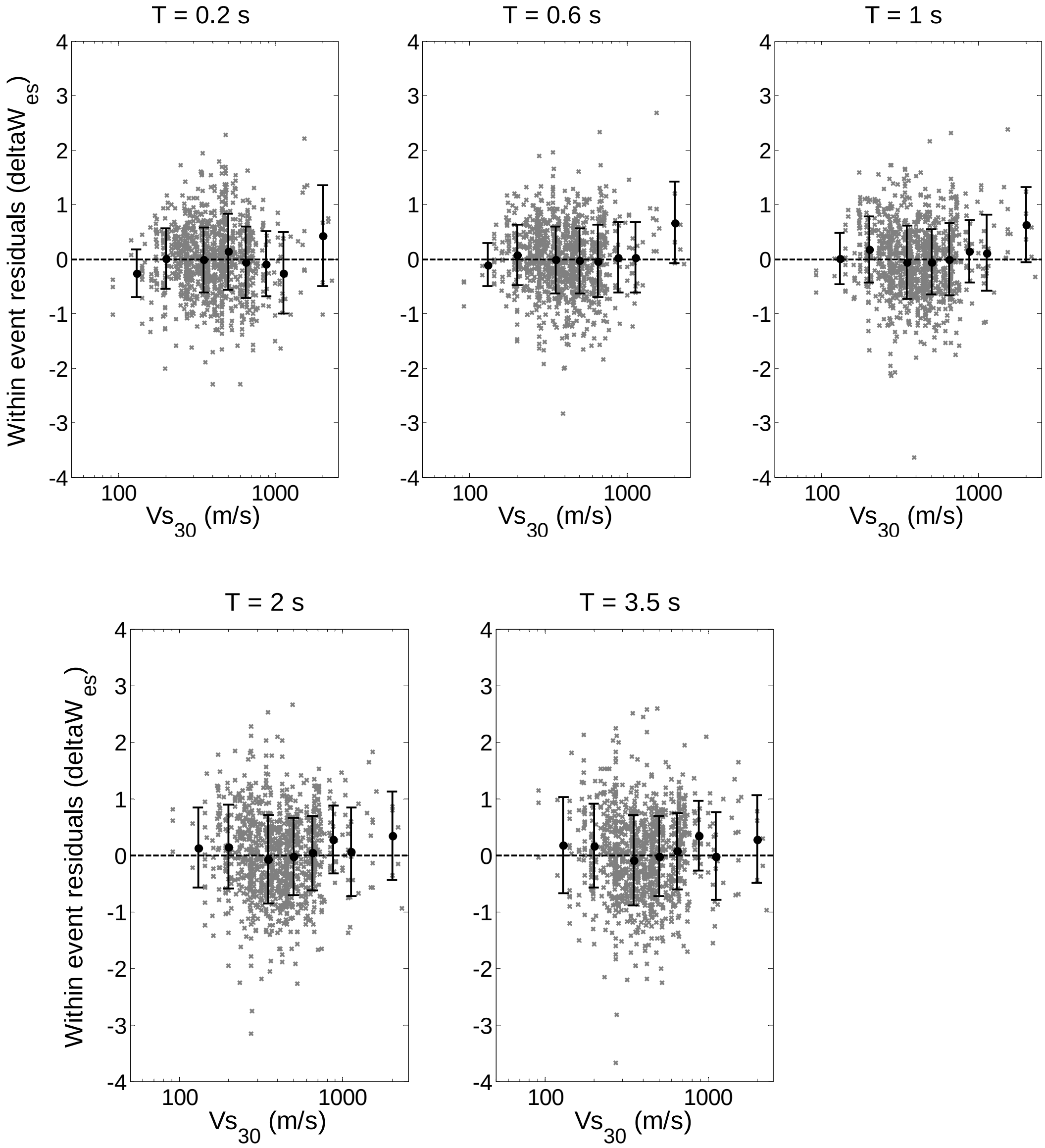


**Figure 12:** Within-event residuals (deltaw$_{es}$ ) and binned averages with respect to $V_{s30}$ at periods 0.2, 0.6, 1 s, 2 s and 3.5 s.

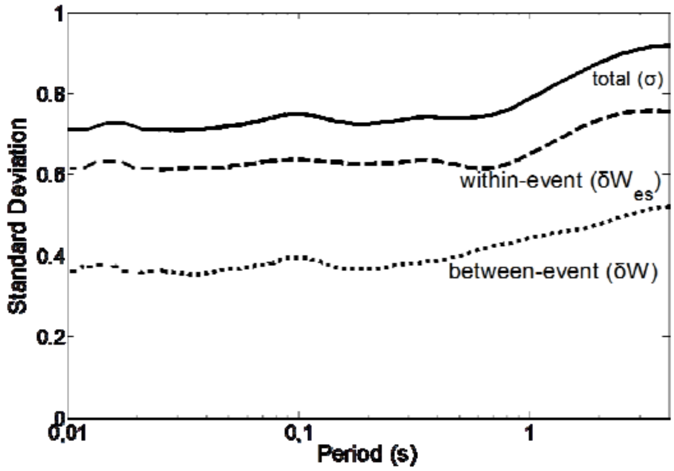


**Figure 13:** Components of the standard deviation of $ASA_{40}$ using the new model.